Electrostatic Calculations of Amino Acid Titration and Electron Transfer, $Q_A^-Q_B \rightarrow Q_AQ_B^-$, in the Reaction Center

P. Beroza, D. R. Fredkin, M. Y. Okamura, and G. Feher
Department of Physics, University of California, San Diego, La Jolla, California 92093 USA

ABSTRACT The titration of amino acids and the energetics of electron transfer from the primary electron acceptor (Q_A) to the secondary electron acceptor (Q_B) in the photosynthetic reaction center of *Rhodobacter sphaeroides* are calculated using a continuum electrostatic model. Strong electrostatic interactions between titrating sites give rise to complex titration curves. Glu L212 is calculated to have an anomalously broad titration curve, which explains the seemingly contradictory experimental results concerning its pK_a. The electrostatic field following electron transfer shifts the average protonation of amino acids near the quinones. The pH dependence of the free energy between $Q_A^-Q_B$ and $Q_AQ_B^-$ calculated from these shifts is in good agreement with experiment. However, the calculated absolute free energy difference is in severe disagreement (by ~230 meV) with the observed experimental value, i.e., electron transfer from Q_A^- to Q_B is calculated to be unfavorable. The large stabilization energy of the Q_A^- state arises from the predominantly positively charged residues in the vicinity of Q_A in contrast to the predominantly negatively charged residues near Q_B. The discrepancy between calculated and experimental values for $\Delta G(Q_A^-Q_B \rightarrow Q_AQ_B^-)$ points to limitations of the continuum electrostatic model. Inclusion of other contributions to the energetics (e.g., protein motion following quinone reduction) that may improve the agreement between theory and experiment are discussed.

INTRODUCTION

The reaction center (RC) is a membrane-bound protein in photosynthetic bacteria that initiates the conversion of light energy into chemical energy by mediating the transfer of two optically excited electrons and two protons to a quinone, Q_B, which is bound to the RC:

$$Q_B + 2e^- + 2H^+ \overset{h\nu}{\rightarrow} Q_BH_2 \qquad (1)$$

The reduced quinone (Q_BH_2) leaves the RC (Crofts and Wraight, 1983; McPherson et al., 1990) and diffuses through the lipids in the bacterial membrane, where it is re-oxidized by the cytochrome bc_1 complex. The net result of these reactions is the transport of protons from the cytoplasm to the periplasm, thus establishing the electrochemical gradient that drives ATP synthesis (reviewed by Cramer and Knaff, 1990).

The first optically excited electron is transferred from the primary electron donor (D), a bacteriochlorophyll dimer, via an intermediate acceptor (bacteriopheophytin) to the primary and secondary electron acceptors (Q_A and Q_B), which, in the RC of *Rhodobacter sphaeroides*, are both ubiquinone-10 molecules. Following re-reduction of the dimer by exogenous cytochrome, a second electron is transferred to Q_B by the same route.

Although Q_B is not protonated until the transfer of the second electron (see Okamura and Feher (1992) for a detailed discussion), the coupling of electron and proton transfer begins with the transfer of the first electron:

$$DQ_AQ_B \overset{h\nu}{\rightleftharpoons} D^+Q_A^-Q_B \overset{\Delta G}{\rightleftharpoons} D^+Q_AQ_B^- \qquad (2)$$

Reduction of either quinone results in an increase in the net protonation of the RC (not shown in Eq. 2), although neither quinone is protonated directly (Maroti and Wraight, 1988; McPherson et al., 1988). Furthermore, proton uptake associated with reduction of Q_B is greater than that for Q_A, which gives rise to a pH dependence of the free energy difference between the two quinone redox states (i.e., $Q_A^-Q_B$ and $Q_AQ_B^-$). Understanding the proton uptake associated with electron transfer is important because it affects electron transfer energetics, and it is likely that this proton uptake is also associated with the protonation of Q_B.

Several experiments have addressed the protonation and electron transfer in RCs. Electron transfer between Q_A and Q_B affects the solution pH (protons are taken up from solution by the RC) and the optical absorption of RC cofactors and amino acids (interactions with the electron shift absorbance bands). These changes provide means of experimentally examining the electron transfer reaction. The identification of important residues in electron transfer and proton uptake comes from experimental measurements on RCs that have been altered by site-directed mutagenesis (for reviews, see Okamura and Feher (1992) and Feher et al. (1992)). The approach has been to replace a titratable amino acid with a non-titratable residue and to compare the electron and proton transfers in the mutant with those observed in the wildtype RC.

This paper addresses theoretical aspects of the changes in protonation of interacting residues in the RC and the energetics associated with the single electron reduction of Q_A and Q_B. We apply a continuum electrostatic model (Bashford and

Received for publication 14 December 1994 and in final form 15 March 1995.

Address reprint requests to George Feher, Dept. of Physics, University of California-San Diego, 0319, 9500 Gilman Dr., La Jolla, CA 92093-0319. Tel.: 619-534-4389; Fax: 619-534-0173; E-mail: simone@sdphul.ucsd.edu.

P. Beroza's present address is Department of Molecular Biology, The Scripps Research Institute, La Jolla, CA 92037.

0006-3495/95/06/2233/18 $2.00

Karplus, 1990; Yang et al., 1993) to investigate the titration of amino acids in the RC when the quinones are in their neutral and reduced states and compute the electrostatic component of the free energy of electron transfer. The calculations are based on the crystallographic structure of the RC from *Rb. sphaeroides* (Allen et al., 1987a,b). The continuum electrostatic model was used to compute energies of different protonation and redox states; statistical averages for titration, proton uptake, and electron transfer equilibrium were obtained by Monte Carlo sampling (Beroza et al., 1991), with special procedures used to sample the quinone redox states.

We begin the investigation of electron transfer energetics by calculating the titration curves for the amino acids in the RC in which both quinones are in their neutral state. We concentrate on the titration of residues that are near the quinone binding sites (Fig. 1), because they will have the strongest influence on electron transfer between the quinones. Next, we calculate the amino acid pK_a shifts resulting from reduction of the quinones, from which the pH dependence of the free energy of electron transfer is obtained. We then include the electron transfer states in the statistical analysis and compute the equilibrium between the electron transfer states $Q_A^- Q_B$ and $Q_A Q_B^-$, from which the absolute free energy of electron transfer is obtained. The effect of site-specific mutation of acidic residues near Q_B is also explored. At each stage of the calculations, experimental results are reviewed and compared with computational results.

COMPUTATIONAL MODEL

To investigate the energetics of electron transfer and proton uptake in the RC we use a continuum electrostatic model. In this model the protein is treated as a set of point charges (representing the charges and polar bonds of the amino acids) that are inside a low-dielectric continuum (the protein), which is embedded in a high dielectric continuum (the solvent). The electrostatic energy of a charge distribution in the protein is determined from the electrostatic potential within the protein, which is calculated by solving the Poisson-Boltzmann equation (McQuarrie, 1976). Initially applied to spherical geometries (Tanford and Kirkwood, 1957), the model has recently been extended to arbitrary geometries through the application of numerical methods (Warwicker and Watson, 1982; Davis and McCammon, 1990; Sharp and Honig, 1990; Gilson and Honig, 1988). This has allowed an atomic level of detail in calculations of electrostatic potentials within proteins. (Methods that model atomic polarization as induced point dipoles (see, for example, Warshel & Russel (1984)) also maintain this level of detail, although it is computationally feasible to treat only limited regions of a protein in this manner.) Several workers have applied the continuum model to calculate the pK_a of amino acids in proteins (Bashford and Karplus, 1990; Yang et al., 1993; Bashford and Gewert, 1992; Oberoi and Allewell, 1993). We applied the finite-difference method to this problem as discussed in a separate paper (Beroza and Fredkin, manuscript submitted for publication).

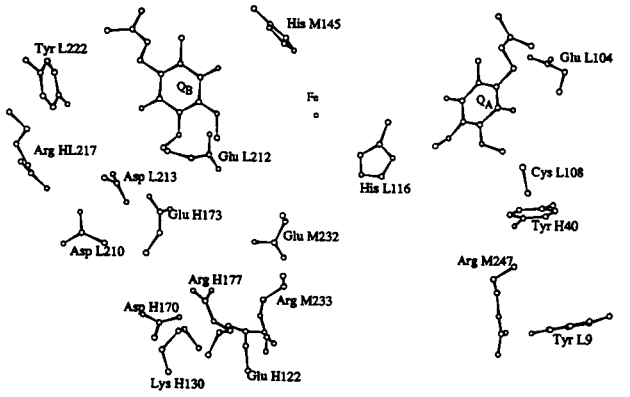

FIGURE 1 The positions, as determined by x-ray crystallography (Allen et al., 1987a,b) of the quinones, Q_A and Q_B, the iron, and the sidechains of nearby titratable residues that, when ionized, have an interaction energy >50 meV with either reduced quinone. A number of acidic residues near Q_B have been shown experimentally to influence electron transfer to Q_B (Okamura and Feher, 1992).

We describe the application of the continuum electrostatic model to the 1) calculation of the titration curves of individual amino acids in the RC when quinones are neutral, 2) calculation of the change in protonation (proton uptake) of the amino acids for the two redox states Q_A^- and Q_B^-, and 3) calculation of free energy of electron transfer.

Calculation of amino acid titration

It is convenient to separate the pK_a of a titrating amino acid residue (we consider the titratable amino acids to be aspartic and glutamic acids, histidine, cysteine, tyrosine, lysine, and arginine) that is bound to a protein into two parts: the intrinsic pK_a (pK_{int}) and the effect of site-site interactions. The intrinsic pK_a is defined as the pK_a a residue would have if all other titrating sites were held in their neutral state (Tanford and Roxby, 1972), and which is, therefore, independent of the protonation state of other titrating sites. The effect of site-site interactions depends on which of the interacting sites are charged, and is, therefore, dependent on the protonation state of other titrating sites.

Single-site titration

The transfer of the amino acid from solution to the protein shifts the energies of its two protonation states, which causes a shift in the pK_a of the residue from its value in solution. If we assume other titrating sites are in their neutral state, this shift gives the intrinsic pK_a of the residue:

$$pK_{int} = pK_s + \Delta pK, \tag{3}$$

where pK_s is the pK_a of the residue in solution (known experimentally) and ΔpK is the pK_a shift, which is related to the free energies of the protonation states in solution and in protein (see Fig. 2) by:

$$\Delta pK = -\frac{1}{k_B T \ln 10}\left(\Delta G^{AH^+}_{s\to p} - \Delta G^{A}_{s\to p}\right), \tag{4}$$

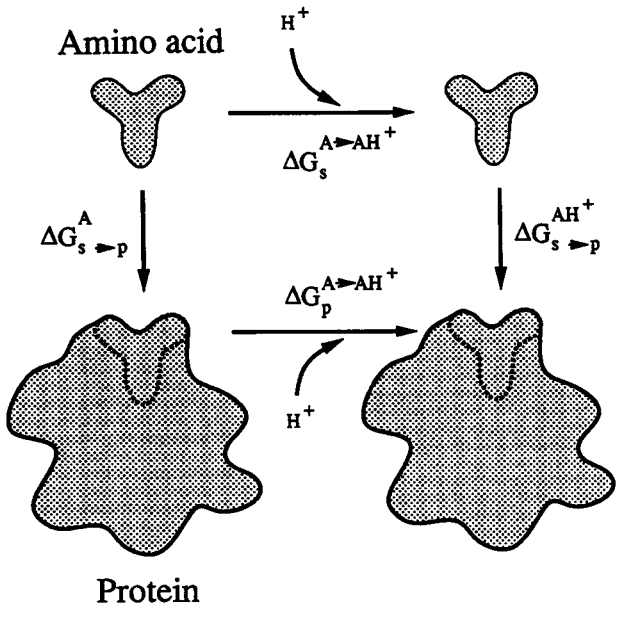

FIGURE 2 Thermodynamic cycle for titration calculation. The change in pK_a when the amino acid is bound to the protein is proportional to the difference $\Delta G^{AH^+}_{s\to p} - \Delta G^{A}_{s\to p} = \Delta G^{A\to AH^+}_{p} - \Delta G^{A\to AH^+}_{s}$, where the subscripts s and p refer to solution and protein, respectively. In our model, we assume this energy difference to be entirely electrostatic in origin.

where the subscripts refer to solution (s) and protein (p). The difference in the free energy associated with protonation of an amino acid that it is bound to the protein from its value in solution is given by:

$$\Delta G^{AH^+}_{s\to p} - \Delta G^{A}_{s\to p} = \Delta G^{A\to AH^+}_{p} - \Delta G^{A\to AH^+}_{s}. \quad (5)$$

The quantities on the right side of Eq. 5 are calculated for each titratable residue in the protein using continuum electrostatic theory, from which the pK_{int} for each residue is obtained from Eqs. 3 and 4.

The origins of the shifts in pK_a from their values in solution lie in the difference between the interactions that the two states of the amino acid have with the protein, solvent, and counterions. In our model, we assume these differences to result from electrostatics. There are clearly other energies (besides electrostatic) that are associated with the transfer of an amino acid from solution to protein. For example, the amino acid forms chemical bonds with the flanking amino acids on the polypeptide chain. The assumption is that these changes are the same for both protonation states, e.g., the bonds formed when the residue is incorporated into a polypeptide chain are far enough away from the protonation site so that these energies are unaffected by titration. Thus, the ΔpK caused by the protein results from the altered electrostatic environment of the residue when it is bound to the protein. This energy has two sources.

1) ΔpK_{solv} (solvation). Interactions with the polarization that the amino acid induces in dielectric media and the interactions with the counterions that redistribute in response to the electrostatic field of the amino acid.

2) ΔpK_{bg} (background). Interactions with polar bonds and permanent charges when all other titrating sites are neutral (note that this includes the effect of the polar bonds in the neutral titrating sites).

Multiple-site titration

The titration of an amino acid bound to a protein is influenced by the protonation state of other titrating sites, which are not taken into account in the calculation of the intrinsic pK_a discussed in the previous section. The net effect of other titrating sites on the pK_a of a residue is statistical, and we must consider all accessible states of the system when computing the average protonation of a titrating residue. In defining accessible states of the protein we make four major assumptions: 1) the electrostatic energies of the different protonation states of the protein are not affected by protein motion and may be calculated from the static x-ray structure; 2) the state of a protein is uniquely defined by the protonation state of each titratable residue; 3) the change in pK_a of an amino acid when it is bound to a protein is entirely electrostatic in origin; and 4) the dielectric response of the protein and solvent is approximately that of a dielectric continuum, and the distribution of counterions is given by the Debye-Hückel theory.

Given these restrictions, the state of a protein can be defined by a vector $\mathbf{x}$ whose elements specify the number of protons bound to each titrating site (either 0 or 1). Thus, for a protein with N titrating sites, a state is defined by a vector of dimension N:

$$\mathbf{x} = (x_1, x_2, ..., x_N),$$

where x_i is the protonation state of site i. The average protonation of a site, $\langle x_i \rangle$, is found by a statistical average (Boltzmann weighted sum) of all protonation states of the protein:

$$\langle x_i \rangle = \frac{\sum_{\{\mathbf{x}\}} x_i e^{-G(\mathbf{x})/k_B T}}{Z}, \quad (6)$$

where x_i is the protonation state of site i when the protein is in protonation state $\mathbf{x}$, $G(\mathbf{x})$ is the free energy of protonation state $\mathbf{x}$, Z is the partition function ($Z = \Sigma_{\{\mathbf{x}\}} e^{-G(\mathbf{x})/k_B T}$), k_B is Boltzmann's constant, T is the temperature, and the sum is over all possible protonation states. Thus, the average protonation of a titrating residue is a statistical problem that involves all the protonation states of the protein. Therefore, the titration of a residue is not easily defined by a single number (pK_a), and the resulting titration curve is often quite different from a classical single-site titration curve (i.e., Fig. 2 and consequently Eqs. 4 and 5 are inadequate for multiple-site titration). We define the pK_a of a residue as the pH at which $\langle x_i \rangle = [1/2]$.

Calculation of the average protonation of a titrating site separates into two parts: 1) calculating the free energy, $G(\mathbf{x})$, for any given protonation state $\mathbf{x}$; and 2) calculating the Boltzmann average (Eq. 6) for the 2^N states of the protein. When these steps are carried out for different pH values, titration curves for the residues are obtained.

Calculation of G(x)

To evaluate Eq. 6, one needs to determine $G(\mathbf{x})$ for any protonation state $\mathbf{x}$. The method we used for calculating the energy of a protein microstate is similar to that described previously (Bashford and Karplus, 1990; Yang et al., 1993). An intrinsic pK_a is calculated for each titrating residue and a matrix of interactions between charged titrating sites is calculated. The energy of a protonation state $\mathbf{x}$ is:

$$G(\mathbf{x}) = \sum_{i=1}^{N} x_i(-k_B T \ln 10)(pK_{int,i} - pH) + \frac{1}{2}\sum_{\substack{i,j=1 \\ i\neq j}}^{N} q_i q_j W_{i,j}, \quad (7)$$

where $pK_{int,i}$ is the intrinsic pK_a of site i, q_i is the charge on site i (i.e., $q_i = x_i$ for cationic sites and $q_i = x_i - 1$ for anionic sites) and $W_{i,j}$ is the interaction energy associated with charging sites i and j (see Yang et al. (1993) for discussion).

The intrinsic pK_as and site-site interaction matrix ($\mathbf{W}$) are calculated from continuum electrostatic theory. For a given protonation state $\mathbf{x}$, the charge distribution in the protein is fixed, and in the continuum model, the electrostatic energy is determined by the electrostatic potential at these charges, which is specified by: 1) the dielectric constant, $\epsilon(\mathbf{r})$, within the region; 2) the distribution of free charge, $\rho(\mathbf{r})$, in the region; and 3) the boundary conditions for the potential on the surface enclosing the region. The details of the calculation of electrostatic energy will be presented elsewhere (P. Beroza and D. R. Fredkin, submitted for publication) and are similar to those used by other workers (Bashford and Karplus, 1990; Yang et al., 1993).

We used the RC coordinates (prerelease structure P4RCR, date 09-SEP-91, resolution of 2.8 Å with an R value of 0.227) as deposited in the Brookhaven Protein Data Bank (Bernstein et al., 1977). Some residues near the amino and carboxy termini of the subunits are omitted from the structure because they could not be reliably located in the electron density. Of these, six are titratable residues (Glu M2, Tyr M3, Asp H11, Lys H249, Glu H258, and Tyr H259), which, in addition to the carboxy and amino termini of the three subunits, make a total of 12 titrating sites that are omitted from our model. In addition, the ligands to the iron were considered to be part of the non-titrating amino acids. The histidine ligands were assumed neutral, and the glutamic acid (M234) was assumed ionized. With these restrictions and the omission of the unresolved titrating sites, the number of titrating sites is reduced from 172 to 155.

The coordinates of the heavy atoms (i.e., non-hydrogen atoms) were taken from the Protein Data Bank. Hydrogen atoms were added using the computer program InsightII (Biosym Technologies, San Diego, CA). Where possible, positions of polar hydrogens near the quinones were adjusted by hand to optimize hydrogen bonding. A solvent probe of radius 1.4 Å was used to define the molecular surface (Richards, 1977; Connolly, 1983), which separates the protein dielectric from the solvent dielectric. Ionic strength was 50 mM KCl, in accord with experimental conditions used for measuring proton uptake (McPherson et al., 1988). The solvent dielectric constant was taken to be 80 and the protein dielectric constant 4 (see Harvey (1989), Gilson and Honig (1986) for discussion of the choice of dielectric constant of a protein).

The charge distribution of the amino acids in the protein were taken from the DISCOVER parameter set (Hagler et al., 1973). The cofactors were considered entirely apolar (i.e., all partial charges set to 0), with the following exceptions. 1) All carbonyl bonds in the cofactors (including the quinones in the unreduced state) were assigned a partial charge of $+0.38e$ on the carbon and $-0.38e$ on the oxygen, consistent with the carbonyl bonds in the protein. 2) The $+2e$ charge on the non-heme iron was delocalized over the iron-histidine complex, with $+0.7e$ localized on the iron and $+1.3e$ distributed evenly over the heavy atoms of the four imidazole rings that are ligands to the iron. This charge distribution on the iron-histidine complex is based on calculations of the electronic structure of metal-imidazole complexes (L. Noodleman, C. Fisher, and J. Li, personal communication). Delocalization of the negative charge of the glutamate over the iron complex had little effect on the results. 3) The negative charge on the reduced quinone was distributed with ⅓ on each carbonyl oxygen and ⅓ spread evenly over the six carbons of the quinone ring.

The atomic van der Waals radii used in the calculations (see Table 1) were taken from Yang et al. (1993). The van der Waals radii used for the continuum electrostatic calculations are similar to those of the PARSE parameter set (Sitkoff et al., 1994), which has been optimized to reproduce small molecule solvation energies from a continuum electrostatic model that uses the partial charges from DISCOVER (Hagler et al., 1973).

Calculation of thermal averages

Evaluation of the Boltzmann sum in Eq. 6 presents a problem for all but the smallest proteins, as the number of terms in the sum grows exponentially with the number of titrating sites. Consequently, computing the complete sum exactly is only feasible for small proteins, such as lysozyme (Bashford and Karplus, 1990). For larger proteins, approximation methods must be employed. The mean-field approximation for multiple-site titration (Tanford and Roxby, 1972) has been shown to fail for strongly coupled sites (Bashford and Karplus, 1991). Methods that either discard some of the unlikely states in the partition function (Bashford and Karplus, 1991) or treat clusters of interacting sites exactly and use the mean-field approximation for interactions between sites in different clusters (Yang et al., 1993; Gilson, 1993) have been found to be successful in calculating the sum for most proteins. However, for a protein as large as the RC, which has large clusters of strongly interacting sites, these methods fail. We have demonstrated that Monte Carlo sampling of protonation states gives reliable titration curves for very large proteins with strongly interacting sites (Beroza et al., 1991). We use this method to determine the titration curves presented here.

The intrinsic pK_as and the matrix of site-site interactions in Eq. 7 were calculated for all titrating sites in the RC that were resolved in the x-ray structure. The titration behavior of these residues was determined by Monte Carlo sampling of the protonation states of the protein by varying the pH from 0 to 15 in 0.5 pH increments.

Calculation of proton uptake associated with the reduction of the quinones

Calculating the proton uptake resulting from reduction of either quinone involves two separate calculations of the net protonation of the RC, one with the quinone neutral, the other with the quinone negatively charged. The average net protonation of the RC is given by:

$$\langle x_{tot} \rangle = \langle \sum_{i=1}^{N} x_i \rangle, \tag{8}$$

where $\langle x_i \rangle$ is the average protonation of site i, and N is the total number of titrating sites. The change in net protonation of the RC that results from electron transfer to Q_A is then given by:

$$\Delta H^+(Q_AQ_B \rightarrow Q_A^-Q_B) = \langle x_{tot} \rangle_{Q_A^-Q_B} - \langle x_{tot} \rangle_{Q_AQ_B}, \tag{9}$$

where $\langle x_{tot} \rangle_{Q_A^-Q_B}$ is the average net protonation of the RC when Q_A is reduced and $\langle x_{tot} \rangle_{Q_AQ_B}$ is the average net protonation of the RC when Q_A is neutral. The proton uptake for reduction of Q_B is given by a similar equation. Henceforth, when we refer to proton uptake, we mean the quantity in Eq. 9 rather than changes in protonation that are associated with changes in pH (i.e., titration).

Calculation of free energy of electron transfer

ΔG *from proton uptake*

The free energy difference between $Q_A^-Q_B$ and $Q_AQ_B^-$ is related to the proton uptake by the thermodynamic relation (McPherson et al., 1988):

$$\Delta G(Q_A^-Q_B \rightarrow Q_AQ_B^-) = k_BT \ln 10 \times \int_{pH_1}^{pH_2} \Delta[H^+](Q_A^-Q_B \rightarrow Q_AQ_B^-) d\mathrm{pH} + \Delta G_{pH_1}, \tag{10}$$

where ΔH^+ is the net proton uptake by the RC upon electron transfer from Q_A to Q_B, and ΔG_{pH_1} is an integration constant (i.e., the free energy of electron transfer at the lower limit of integration). Note that this method gives the free energy difference only to within an integration constant.

ΔG *from equilibrium population of* $Q_A^-Q_B$

In the calculation of the free energy difference from the integral of the proton uptake (Eq. 10), thermal averages of protonation of amino acids were calculated for fixed quinone redox states (i.e., Q_AQ_B, $Q_A^-Q_B$, and $Q_AQ_B^-$). An alternative method for determining the free energy difference allows the redox states to vary in the thermal average in the same way protonation states are allowed to vary. This modification to the model, in which the redox states of the quinones are included in the statistical distribution, allows us to calculate the relative population of the $Q_A^-Q_B$ state in the $Q_A^-Q_B \leftrightarrow Q_AQ_B^-$ equilibrium. The free energy is obtained from the thermodynamic relation (Kleinfeld et al., 1984):

$$\Delta G(Q_A^-Q_B \rightarrow Q_AQ_B^-) = k_BT \ln \frac{\alpha}{1-\alpha}, \tag{11}$$

where α is the partition coefficient, given by:

$$\alpha = \frac{[Q_A^-Q_B]}{[Q_A^-Q_B] + [Q_AQ_B^-]}. \tag{12}$$

Unlike the method of integrating the proton uptake, which gives the pH dependence of the free energy difference only up to an undetermined integration constant, this method allows direct calculation of the absolute free energy difference. Because charge recombination between Q_B^- and the oxidized donor (D^+) was shown to proceed indirectly via a thermal population of Q_A^- (Kleinfeld et al., 1984), α and ΔG are related to the charge recombination rate by:

$$k_{BD} = \alpha k_{AD} = k_{AD}/(1 + e^{-\Delta G/k_BT}), \tag{13}$$

where k_{AD} and k_{BD} are the charge recombination rates between the primary donor, D^+, and Q_A^- and Q_B^-, respectively. From the calculated value of α and the experimentally measured value for k_{AD}, k_{BD} can be calculated from Eq. 13 and compared with the experimentally measured value.

Sampling electron transfer states

To obtain the partition coefficient, α, from which ΔG is obtained by Eq. 11, we apply the continuum electrostatic model to the quinone redox states. The same thermodynamic cycle that was used for amino acid protonation (Fig. 2) is used, but instead of the protonation state the redox state is changed. The same approximation made for amino acid titration is made for quinone reduction: the redox potential of a quinone bound to the RC is equal that of a quinone in solution plus an electrostatic shift caused by the protein environment. As in the case of an amino acid, the electrostatic energy of a quinone can be divided into two parts: 1) ΔG°_{int}, the "intrinsic

TABLE 1 Atomic van der Waals radii used to calculate the dielectric interface between protein and aqueous solution (Yang et al., 1993)

Atom	Radius (Å)
C	1.9
N	1.65
O	1.6
H	1.0
S	1.9
Mg	1.75
Fe	1.95

redox potential" (in analogy to the intrinsic pK_a of an amino acid), which is the redox potential in solution plus the electrostatic interaction with the non-titrating charges in the protein and 2) ΔG°_{titr}, which results from the electrostatic interactions with titrating sites. Note that the redox potential of a quinone is not directly coupled to the protons in solution, but is indirectly coupled to them through its interactions with titrating sites.

Incorporating the redox states of the quinones into the statistical mechanical analysis is straightforward. The dimension of the state vector is increased by two: $\mathbf{x} = (x_a, x_b, x_1, x_2, \ldots x_N)$, where x_a and x_b represent the redox state of Q_A and Q_B (1 = reduced, 0 = neutral). The **W** matrix of site-site interactions (see Eq. 7) is also increased to include the interactions between the quinones and the titrating sites. Only one electron is transferred between the quinones, and, therefore, only one electron is allowed in the Monte Carlo sampling. Thus, only the $Q_A^- Q_B$ and $Q_A Q_B^-$ states are sampled, while the $Q_A Q_B$ and $Q_A^- Q_B^-$ states are not.

The total number of accessible states of the protein is increased, and the partition coefficient (i.e., the average population of the $Q_A^- Q_B$ state) is given by

$$\alpha = \langle x_a \rangle = \frac{\sum_{\mathbf{x}} x_a e^{-\beta G(\mathbf{x})}}{Z}, \qquad (14)$$

where $x_a = 1$ when the electron is on Q_A and 0 otherwise. Thus, the calculation of α, the average redox state of Q_A, is very similar to the calculation of $\langle x_1 \rangle$, the average protonation state of a titrating site (see Eq. 6). The only difference is that, when calculating α, the redox states of Q_A and Q_B are included in the state vector **x**.

Non-Boltzmann sampling

Initial calculations showed that only one redox state ($Q_A^- Q_B$) was significantly populated. The relative population of the $Q_A Q_B^-$ state was small (<0.1), which prevented accurate sampling of the protonation states when the electron was on Q_B. To get around this sampling problem we use a non-Boltzmann sampling technique (Chandler, 1987) which biases the Monte Carlo trajectory to insure that both quinone states are well sampled. For a given pH, a constant G_{bias} is subtracted from the redox energy of the $Q_A Q_B^-$ state, which artificially lowers the energy of $Q_A Q_B^-$ (i.e., G_{bias} depends only on the location of the electron and not on the protonation state). The free energy driving the sampling, G_{samp}, is related to the true free energy of the system, G_{real}, by $G_{real} = G_{samp} + G_{bias}$. The energy bias is adjusted until $\alpha \approx \frac{1}{2}$. Forcing the electron to reside on Q_B half of the time improves the sampling of the states of the protein in which the electron is on Q_B. However, the energy bias skews the distribution of states in favor of the unlikely $Q_A Q_B^-$ states; as a result, the sampled set no longer obeys the correct Boltzmann distribution.

To correct for the error introduced by the bias, the computed averages of the sampled $Q_A Q_B^-$ states are reduced by the Boltzmann factor of the energy bias. The correct averages are obtained by separating the Boltzmann factor in Eq. 14:

$$\alpha = \langle x_a \rangle = \frac{\sum_{\mathbf{x}} \{x_a e^{-G_{bias}(\mathbf{x})/k_B T} e^{-G_{samp}(\mathbf{x})/k_B T}\}}{\sum_{\mathbf{x}} \{e^{-G_{bias}(\mathbf{x})/k_B T} e^{-G_{samp}(\mathbf{x})/k_B T}\}} \qquad (15)$$

which is the same as Eq. 14, but the Boltzmann factor has been separated and the partition function has been written explicitly.

The numerator and denominator correspond to statistical averages over the free energy G_{samp}. Thus, we can drive the Monte Carlo sampling according to G_{samp} but evaluate a weighted average to obtain α:

$$\alpha = \frac{\langle x_a e^{-G_{bias}(\mathbf{x})/k_B T} \rangle_{samp}}{\langle e^{-G_{bias}(\mathbf{x})/k_B T} \rangle_{samp}} \qquad (16)$$

where the brackets represent averages from the biased Monte Carlo sampling. This non-Boltzmann sampling increases the accuracy of the calculated ΔG values by sampling the $Q_A Q_B^-$ states more accurately.

Modeling mutant RCs

An important goal of these calculations is to determine the effect of site-directed mutagenesis on the experimentally measured value of k_{BD}, the charge recombination rate, which probes the free energy of electron transfer between Q_A and Q_B. In the calculations, the recombination rate was determined from the experimental value of k_{AD} and the calculated value of α by using Eq. 13. The mutants studied were those in which an acidic residue (Glu or Asp) was replaced by its non-titrating analog (Gln or Asn). Site-directed mutagenesis was simulated by changing the intrinsic pK_a of the mutated residue to force it to be always neutral. The two main approximations made in the calculations for mutated RCs are that 1) the structure of the RC is not affected by the mutation, and 2) the titrating acid in its neutral (protonated) form is equivalent to the non-titratable residue to which it is mutated (i.e., a protonated Glu is equivalent to a Gln). Although the charge distributions on the neutral acid and the non-protonatable mutants have different dipole moments, the effect of this difference is expected to be small compared with the change in net charge on the residue. The charge recombination rates were calculated by the following procedure:

1) The partition coefficient α (i.e., the fractional population of the $Q_A^- Q_B$ state) at pH = 7 was calculated for wildtype and mutant RCs by Monte Carlo sampling.

2) $\Delta G(Q_A^- Q_B \rightarrow Q_A Q_B^-)$ at pH 7 was calculated from α using Eq. 11, and the systematic error for wildtype RCs (see below) was subtracted from each result.

3) The pH dependence of $\Delta G(Q_A^- Q_B \rightarrow Q_A Q_B^-)$ for each mutant was calculated by integrating the difference in net protonation of the RC when the electron is transferred from Q_A to Q_B (see Eq. 10).

4) The pH dependence of k_{BD} was calculated from the calculated free energy and the experimental value of k_{AD} and Eq. 13.

TITRATION OF AMINO ACID RESIDUES IN THE RC

Computational results

Before we discuss electron transfer, we examine the titration of amino acids in the RC when both quinones are in their neutral state. The titration curves (the pH dependence of the average protonation of a titrating site) were calculated for all 155 sites that were resolved in the x-ray structure. Although all sites must be included because of the long-range nature of electrostatic forces, the effect of sites near the quinones is most important. We discuss, therefore, only the titration of those nearby residues. The interaction energies between the reduced quinones and nearby titrating residues are shown in Tables 2 and 3.

The interactions in Table 3 tend to be weaker than those reported previously (Gunner and Honig, 1992), and in some cases the difference is large. For example, we calculate an interaction between Asp L210 and Asp L213 of 3.4 pK units compared to 6.2 (Gunner and Honig, 1992). However, the previous calculations (Gunner and Honig, 1992) were based on an earlier refinement of the RC structure. Subsequent recalculation based on the newer structure gives an interaction energy between Asp L210 and Asp L213 of 4.1 pK_a units (M. Gunner, personal communication), which is in better agreement with our result. The remaining discrepancies result from their use of slightly different atomic radii and partial charges and their approximation to the molecular surface that appears to slightly overestimate the region of low dielectric constant, resulting in larger interactions between charged sites (M. Gunner, personal communication).

As described above, the titration of a residue is influenced by three factors: solvation (ΔpK_{solv}), background interactions (ΔpK_{bg}), and interactions with charged titrating sites. In the continuum model, the dielectric constant near the titrating site in the protein is lower than in solution. As a result, ΔpK_{solv} shifts the pK_a to favor the neutral form of the residue. The size of this shift depends on how deeply the residue is buried in the low dielectric of the protein, and for residues near the quinone binding sites, this shift is several pK_a units. However, the interactions of a residue with dipoles or permanent charges in the protein (ΔpK_{bg}) or with charged titrating sites can offset this shift.

Titration of residues near Q_A

The intrinsic pK_as of residues that have an interaction with Q_A of >50 meV (i.e., >0.8 pK units) are shown in Table 4.

TABLE 2 Site-site interactions* near Q_A^- (in pK_a units)

Residue	Tyr^- H40	Glu^- L104	Cys^- L108	His^+ L116	Arg^+ M247	Tyr^- L9
Q_A^-	2.8	1.9	1.6	−0.9	−0.9	0.9
Tyr^- H40		0.6	0.7	−0.4	−1.4	2.4
Glu^- L104			4.2	−1.0	−0.6	0.4
Cys^- L108				−1.8	−1.2	0.7
His^+ L116					0.6	−0.4
Arg^+ M247						−7.2

*The electrostatic interactions between charged residues and the reduced quinone (i.e., $W_{i,j}$ in Eq. 7).

The sites near Q_A are not well solvated, which results in large shift in pK_a values. For both cationic and anionic sites, the shift favors the neutral form of the residue (i.e., $\Delta pK_{solv} > 0$ for anions and <0 for cations). For Tyr H40, Glu L104, Cys L108, and Tyr L9, the background interactions do little to alter the effect of desolvation, and the very large intrinsic pK_as for these residues suggest that they are neutral throughout the entire experimental pH range unless there are large compensating interactions with other titrating sites. Arg M247 and His L116 have depressed intrinsic pK_as because of loss of solvation. Arg M247 has large (3 pK_a units) compensating interactions with dipoles in the RC. His L116 has no such compensating interactions and is probably neutral in the experimental pH range.

The titration curves, as calculated from the Monte Carlo sampling, for these residues are shown in Fig. 3 *A*. Only Arg M247 is found to titrate significantly below pH 12. The anomalous titration is the result of an interaction with Lys L110, which titrates in the same pH range. The other titrating sites listed in Table 2 remain predominantly neutral throughout the pH range. Thus, aside from Arg M247, there are no charged residues close to Q_A.

Titration of residues near Q_B

The titration of residues near Q_B is much more complicated than those near Q_A. There are two reasons for this. First, there are a larger number of sites that interact strongly with Q_B (see Fig. 1). Second, these sites interact more strongly with each other, complicating the titration behavior of the individual residues.

The intrinsic pK_as of residues that have an interaction with Q_B of >50 meV are shown in Table 5. The most striking feature of Table 5 is the large negative pK_a shifts from background interactions. For acidic sites, these interactions approximately cancel the pK_a shifts caused by desolvation. For cationic sites, such as Arg H177 and Arg M233, these background interactions shift the intrinsic pK_as down, in the same direction as the ΔpK_{solv}. Thus, without considering interactions between titrating sites, the environment (as far as titration is concerned) near Q_B is strikingly similar to aqueous solution for acidic residues.

What is responsible for the background interactions that favor the ionization of the acids near Q_B? One obvious candidate is the iron and its ligands, which carry a net positive charge. This charge would stabilize the negative form of an acid, thereby lowering its pK_a. However, an analysis of the background energy reveals that the iron/ligand complex contributes a relatively small amount to the negative background energies in Table 5. Its largest interaction is with Glu L212, which results in a pK_a shift of ~−2 pK_a units, only ⅓ of the total stabilization. The interaction between the iron/ligand complex with other nearby acids, Asp L213 and Glu H173, is ~−1 pK_a unit, which is only ¼ of the total ΔpK_{bg}.

A large part of the stabilization of acidic residues results from their interactions with peptide bonds in the polypeptide backbone of the RC. The peptide bond has a

TABLE 3 Site-site interactions* near Q_B^- (in pK_a units)

Residue	Glu^- L212	Asp^- L213	Glu^- H173	Arg^+ L217	Glu^- H122	Arg^+ H177	Asp^- H170	Lys^+ H130	Arg^+ M233	Glu^- M232	Tyr^- L222	Asp^- L210	His^+ M145
Q_B^-	4.8	2.9	2.2	−1.2	1.2	−1.2	1.1	−1.1	−1.1	1.1	0.9	0.9	−0.9
Glu^- L212		3.4	2.6	−1.1	2.8	−2.4	2.4	−2.6	−2.6	1.9	0.5	1.4	−0.9
Asp^- L213			4.9	−3.4	2.0	−2.0	2.2	−2.0	−1.8	1.4	0.8	3.4	−0.3
Glu^- H173				−1.8	2.0	−3.1	3.2	−2.2	−2.0	2.2	1.0	1.5	−0.2
Arg^+ L217					−0.6	0.8	−0.9	0.7	0.6	−0.6	−1.0	−2.7	0.2
Glu^- H122						−3.2	3.0	−7.6	−8.7	2.0	0.3	0.9	−0.2
Arg^+ H177							−14.4	5.5	4.4	−3.5	−0.4	−0.9	0.2
Asp^- H170								−6.3	−3.4	2.3	0.4	1.1	−0.2
Lys^+ H130									5.9	−2.0	−0.3	−1.0	0.2
Arg^+ M233										−2.8	−0.3	−0.8	0.2
Glu^- M232											0.4	0.6	−0.2
Tyr^- L222												0.4	−0.1
Asp^- L210													−0.2

*The electrostatic interactions between charged residues and the reduced quinone (i.e., $W_{i,j}$ in Eq. 7).

TABLE 4 Intrinsic pK_as of residues that have an interaction of >50 meV with Q_A^-

Residue	pK_{soln}*	ΔpK_{solv}‡	ΔpK_{bg}§	pK_{int}¶
Tyr H40	9.6	9.9	−3.9	15.6
Glu L104	4.4	8.2	1.4	14.0
Cys L108	8.3	9.4	2.3	20.0
His L116	6.3	−4.2	−0.7	1.4
Arg M247	12.5	−7.4	3.0	8.1
Tyr L9	9.6	11.6	5.8	27.0

*pK_{soln}, pK in solution.
‡ΔpK_{solv}, shift in pK_a resulting from solvation.
§ΔpK_{bg}, shift in pK_a resulting from background interactions.
¶pK_{int}, the intrinsic pK_a is the pK_a a residue would have in the protein if all other titrating sites were in their neutral states; it is given by $pK_{int} = pK_{soln} + \Delta pK_{solv} + \Delta pK_{bg}$.

permanent dipole moment, and when this moment is directed toward a negative charge, the interaction energy is negative and, therefore, stabilizing. The structural motifs in the RC that are responsible for orienting peptide dipoles to stabilize negative charge near Q_B have been described by Gunner and Honig (1992). The four acidic residues that interact most strongly with Q_B (Glu L212, Asp L213, Glu H173, and Glu H122) have interactions with the peptide dipoles that lower their pK_as. The largest contribution is from the transmembrane E helix from the L subunit ($\Delta pK = -1.15$). Although some interactions with specific peptide bonds are large (e.g., the pK_a shift of Glu L212 resulting from the backbone atoms in Gly L225 in the E helix is ~−0.4), much of the stabilization results from the cumulative effect of many oriented dipoles that are up to ~20 Å away from the acids they stabilize. Almost half of the −1.15 pK_a shift of Glu L212 caused by the E helix results from interactions with peptide bonds that are each less than 0.2 pK_a units in magnitude.

Thus, the stabilization of acidic residues near Q_B is mainly the result of interactions with peptide dipoles of the polypeptide backbone of the RC and, to a lesser extent, with the net positive charge of the iron/ligand complex.

Another effect that is very pronounced in the Q_B region is the influence that the titrating residues have on each other. Unlike the sites near Q_A, the interactions between sites in the Q_B region are large (compare Tables 2 and 3). The Q_B region contains a number of cationic sites in proximity to anionic sites, an arrangement that stabilizes the ionized forms of each. These residues have to pay high solvation penalties for their ionized forms, but the interactions with opposite charges compensate for this penalty.

The titration curves, for the residues closest to Q_B, as calculated from the Monte Carlo sampling, are shown in Fig. 3 *B*. Many of the titrating sites near Q_B have fixed protonation states during the entire pH range of the calculation (0–15). All cationic sites listed in Table 3 are protonated and have, therefore, a fixed, positive, charge (Arg L217, Arg H177, Arg M233, Arg H117, and Lys H130). This is remarkable given that many of these residues have intrinsic pK_as which are more than 10 units lower than their pK_as in solution (see Table 5). Anionic sites that interact strongly with these charged cationic sites are also ionized. This mutual stabilization allows the residues to be ionized even though they are poorly solvated.

Of the three acidic residues nearest Q_B, Glu L212 and Glu H173 titrate in the low pH region (see Fig. 3 *B*). The titration of Glu L212 is very gradual; it has an average protonation between 0.1 and 0.9 from pH 2 to pH 9. This is the result of many weak interactions with titrating sites closer to the surface that counteract the effects of pH. Gunner and Honig (1992) calculated Glu L212 to be fully ionized from pH 5 to 11. It has been shown that the calculated titration curve for Glu L212 is very sensitive to variations of the parameters of the continuum electrostatic model (Beroza et al., 1994). The probable cause for the higher pK_a in our calculation is the charge on the non-heme iron, which is distributed over the four histidine ligands; this tends to move positive charge away from Glu L212, thereby stabilizing its protonated state.

Asp L213 has a very peculiar titration curve, with an average protonation that increases with increasing pH. This anomaly results from strong interactions with Asp L210 and Glu L212. As these two residues deprotonate, the unfavorable interaction with the ionized form of Asp L213 raises its pK_a.

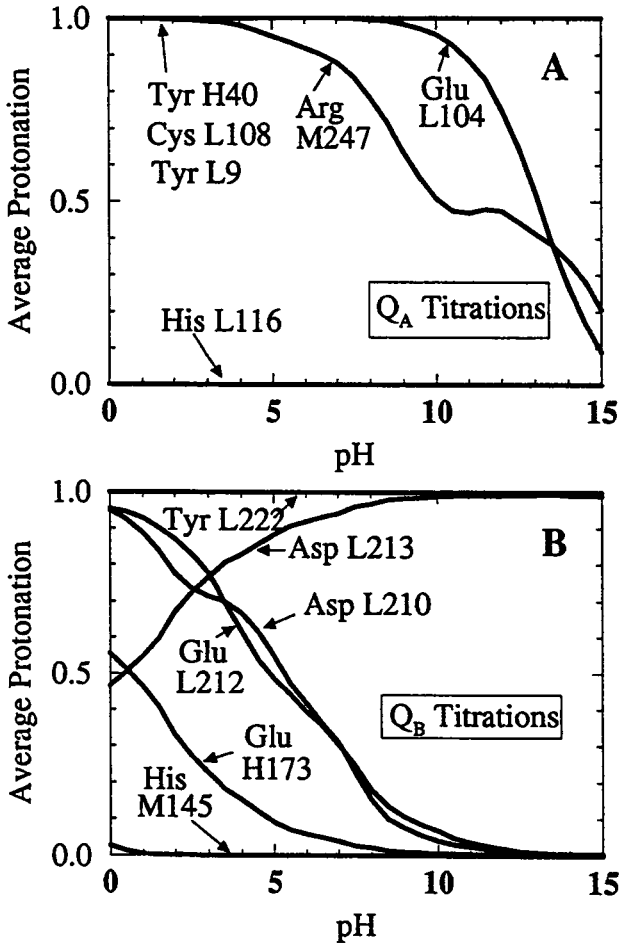

FIGURE 3 Theoretical calculation of titration curves for residues near Q_A (*A*) and Q_B (*B*) that have an interaction energy with the reduced quinone of >50 meV. (*A*) Most residues near Q_A have a fixed protonation state. Glu L104 begins to titrate in the high pH range. Arg M247 has an anomalous titration that begins at pH ~5, while at pH = 15 it is still partially protonated. (*B*) Near Q_B, four acids titrate in the pH range 0–15 (all strongly interacting residues that are not shown are ionized throughout this pH range). All titrations are more gradual than that given by a classical single site titration curve. The protonation of Asp L213 increases with pH as a result of unfavorable interactions with the depronating Asp L210 and Glu L212.

Review of experimental results

Q_B is the ultimate proton and electron acceptor; consequently, experiments have focused on the mutation of residues near Q_B. The two closest residues to Q_B, Glu L212 and Asp L213, have been mutated to glutamine and asparagine, respectively (Paddock et al., 1989, 1990; Takahashi and Wraight, 1992). In addition, Asp L210, which, because of its proximity to Asp L213 and greater exposure to solvent, may be part of a proton transfer chain to the more buried acids L212 and L213 (Beroza et al., 1992), has been mutated to asparagine (Paddock et al., 1992). Other mutants in this region have been constructed, but they involve less conservative structural changes and will not be discussed here. The experimental evidence for the titration of individual residues comes from changes in the charge recombination rate (k_{BD}) for the electron transfer reaction $D^+Q_AQ_B^- \rightarrow DQ_AQ_B$ (to be discussed in a later section). Because glutamine and asparagine are neutral in the pH range for which the RC is stable (pH 4–11), changes in k_{BD} resulting from these mutations have been ascribed to a net charge change from −1 (the ionized acid) to 0 (the neutral amide). The implications of these changes for amino acid titration are summarized in Table 6.

One striking result from the studies of charge recombination in mutated RCs was the effect of the Glu → Gln mutant at position L212. In native RCs, the rate of charge recombination from the reduced quinone to the oxidized primary donor (i.e., $D^+Q_B^- \rightarrow DQ_B$) increases with pH for pH > 9. This is consistent with the titration of an acidic residue near Q_B. Such a titration would introduce a negative charge that would interact unfavorably with the reduced quinone, raising the energy of the $Q_AQ_B^-$ state and increasing the rate of electron transfer from the quinone to the donor. In the L212 Glu → Gln mutant RCs, this pH dependence is absent (Paddock et al., 1989), and the charge recombination rate remains constant with pH. In addition, below pH 9, there is

TABLE 5 Intrinsic pK_as of residues that have an interaction of >50 meV with Q_B^-*

Residue	pK_{soln}	ΔpK_{solv}	ΔpK_{bg}	pK_{int}
Glu L212	4.4	5.7	−6.4	3.7
Asp L213	4.0	4.2	−4.0	4.2
Glu H173	4.4	4.2	−5.4	3.2
Arg L217	12.5	−3.9	0.3	8.9
Glu H122	4.4	5.4	−5.2	4.6
Arg H177	12.5	−4.6	−8.2	−0.3
Asp H170	4.0	4.7	−1.4	7.3
Lys H130	10.4	−7.8	−2.3	0.3
Arg M233	12.5	−4.6	−1.0	6.9
Glu M232	4.4	4.4	−7.0	1.8
Tyr L222	9.6	7.7	1.3	18.6
Asp L210	4.0	3.1	−1.7	5.4
His M145	6.3	−2.7	−1.6	2.0

*Heading definitions are the same as for Table 4.

TABLE 6 Summary of the pK_as of three acidic residues near Q_B, deduced from experimental results on site-directed mutants

Residue	Mutation	Conclusion
L212	Glu → Gln	1) The slope of k_{BD} at high pH is removed, suggesting that Glu L212 titrates in the high pH range (pK_a ~ 9.5) and protonates when Q_B is reduced (Paddock et al., 1989). 2) At pH 7, an infrared spectral line consistent with protonation of a carboxylic acid disappears, suggesting that Glu L212 is ionized at pH 7 (Hienerwadel et al., 1995).
L213	Asp → Asn	The much lower k_{BD} suggests that Asp L213 is ionized for most of the experimental pH range and that its interaction with Q_B^- ~ 60 meV (Paddock et al., 1990).
L210	Asp → Asn	The slope of k_{BD} at low pH is removed, suggesting theAsp L210 titrates in the normal acidic range (~4). The high pH titration observed in this mutant is lower than in wildtype, suggesting an electrostatic interaction between Asp L210 and Glu L212 of ~1.5 pK_a units (Paddock et al., 1992).

little difference in charge recombination kinetics between the wildtype and mutant RCs. This suggests that Glu L212 has a pK of 9.5.

In apparent conflict with the charge recombination results, which indicate a high pK_a for Glu L212, are recent kinetic infrared spectroscopic measurements on wildtype and mutant RCs (Hienerwadel et al., 1995). At pH 7, the difference in infrared (IR) absorption before and after electron transfer to Q_B has a component at 1725 cm^{-1}, consistent with the absorption change associated with protonation of a carboxyl group (i.e., $COO^- + H^+ \rightarrow COOH$). The absorption change at 1725 cm^{-1} is not present in the L212 glutamic acid → glutamine mutant. This suggests that the absorption is caused by the increased protonation of Glu L212 upon reduction of Q_B, which is consistent with a pK of Glu L212 of ~7 or below, in contradiction to the pK_a assigned to Glu L212 on the basis of charge recombination experiments. A possible resolution of these seemingly contradictory experimental results is discussed in the next section.

Mutation of aspartic acid L210 or L213 to asparagine (Paddock et al., 1990, 1992) affected the low pH dependence of the charge recombination rate, which suggests that, in native RCs, these acids deprotonate at low pH, similar to their titration in solution. Mutation of Asp to Asn at the L213 site not only removes the pH dependence below pH 7, but also slows the rate of charge recombination (k_{BD}) by a factor of ~10. This suggests that Asp L213 is ionized in native RCs and interacts unfavorably with the reduced Q_B^-. Upon mutation to Asn, this unfavorable interaction is removed, Q_B^- is more stable, and the recombination rate is slowed. Asp L210, which is farther from Q_B than Asp L213, has a smaller interaction with Q_B^-, and its mutation to Asn has less of an effect on the charge recombination rate. The dependence of k_{BD} at low pH is also removed by this mutation. For both of these mutations the onset of the increase in k_{BD} at high pH is shifted to lower pH. This is consistent with a titration of an acid that undergoes a downward pK_a shift when either Asp L210 or Asp L213 is mutated to Asn.

Comparison of computational and experimental results

Glu L212

The charge recombination experiments on the Glu → Gln mutant suggest that Glu L212 has a pK ~ 9.5 (Paddock et al., 1989), while the kinetic IR results indicate a $pK_a < 7$ (Hienerwadel et al., 1995). A clue to the resolution of this apparent conflict in the pK_a values of Glu L212 is provided by the calculated titration curve. A classical titration curve cannot explain the two experimental results because the average protonation of a residue falls off too quickly with increasing pH. However, the titration curve calculated for L212 is much more gradual than a classical titration curve (see Fig. 3). The electrostatic interactions with other titrating sites broaden the titration curve significantly. Thus, proton uptake at low pH is possible even though at high pH Glu L212 remains protonated in a significant fraction of RCs. However, this explanation is only qualitative. The model does not explain the relatively abrupt pH dependence of the charge recombination kinetics. Our model would predict that mutation of Glu L212 to Gln would alter the pH dependence of k_{BD} at lower pH also, and this is not observed experimentally. Nevertheless, it is clear that titration of residues in the protein interior cannot be described by a single number, the pK_a, and that more complex behavior results from interactions among titrating sites. Such complex titration behavior is likely to be the cause of the experimental results on the pK_a of Glu L212, which clearly disagree when analyzed in terms of a classical titration curve with a single pK_a.

Asp L213

A striking computational result is the increase in average protonation of Asp L213 with increasing pH (see Fig. 3 *B*). This residue is strongly coupled to Glu L212 and Asp L210. As the pH increases, Glu L212 and Asp L210 deprotonate, and their electrostatic interaction with Asp L213, which is ionized at low pH, causes Asp L213 to protonate. Such "inverse titration" has been observed experimentally in an amino-carboxylate compound (Sudmeier and Reilly, 1964), and in calculations of amino acid titration in the RC (Gunner and Honig, 1992) and bacteriorhodopsin (Bashford and Gewert, 1992), which, like the RC, acts as an optically driven proton pump. Although inverse titration curves have been observed experimentally (Sudmeier and Reilly, 1964), in the case of the RC there is no experimental evidence for increasing protonation of Asp L213 with increasing pH. On the contrary, in the mutant in which Asp L213 is replaced by asparagine, the rate of charge recombination ($D^+Q_AQ_B^- \rightarrow DQ_AQ_B$) is lower throughout the experimental pH range, which suggests that Q_B^- is stabilized by the mutation (i.e., that Asp L213 is ionized in the wildtype). Moreover, the pH dependence in the low pH range (3–5), observed in the wildtype RCs, is not present. This suggests that Asp L213 has a pK_a typical for a carboxylic acid in solution (~4).

The experimental results described above suggest that the inverse titration of Asp L213 is probably an artifact of the computational model. Because the protein structure is assumed to be static, the only means of lowering the total energy of the system is by proton binding or release. As the pH is increased, the acidic residues titrate, which creates unfavorable interactions between neighboring negative charges. Two strongly unfavorable electrostatic interactions, Asp L213 ↔ Asp L210 and Asp L213 ↔ Glu L212 (see Table 3), are alleviated by protonation of Asp L213. Alternatively, sidechain motion, rather than reprotonation, may reduce the unfavorable interactions and thereby eliminate the inverse titration behavior. This possibility is not included in the model. Analysis of the crystal structure revealed voids near the acidic residues that could permit significant sidechain reorientation (Beroza et al., 1992).

Asp L210

Asp L210 has a calculated titration curve similar to that for Glu L212 (see Fig. 3 *B*). Protonation of these residues is strongly influenced by their interaction with Asp L213. Experimental measurements on RCs in which Asp L210 has been mutated to asparagine suggest that Asp L210 has a pK_a ~ 4, typical for a carboxylic acid in solution. The calculated titration curve is consistent with the experimental results. Asp L210 starts to deprotonate at low pH, but its titration is more gradual than a classical titration curve. Calculation of the effect of the Asp → Asn mutation at L210 predicts a downward shift in pK_a for Glu L212 of ~2 pK_a units, which is also observed experimentally (Paddock et al., 1989).

PROTON UPTAKE ASSOCIATED WITH ELECTRON TRANSFER

Computational results

Having discussed the titrations of residues near the neutral quinones, we now examine the proton uptake associated with reduction of the quinones. This was calculated from the change in the average net protonation of the RC when the quinone is changed from neutral to charged. Residues that interact with the reduced quinone will have their protonated state stabilized, i.e., their pK_as will be shifted up (provided pK_a shifts at other sites do not offset the shift), resulting in a net proton uptake by the residue. Given the large number of interacting titrating sites in the Q_B region, the effect of nearby titrating sites must be included together with the effect of quinone reduction. This is accomplished by the Monte Carlo sampling, which considers all interactions between sites when calculating thermal averages. The Monte Carlo calculation was made for the three different states, Q_AQ_B, $Q_A^-Q_B$, and $Q_AQ_B^-$. The proton uptake resulting from reduction of either quinone is found by subtracting the total protonation of the neutral state from the reduced state (see Eq. 9).

Proton uptake associated with reduction of Q_A

The calculated proton uptake associated with reduction of Q_A is shown in Fig. 4 *A*. The largest contribution to the uptake below pH 8 comes from the fairly distant Glu L212, which has an interaction with Q_A^- of 0.65 pK_a units. The gradual titration of Glu L212 (see Fig. 3 *B*) causes its proton uptake to occur over a wide pH range. Above pH 8 proton uptake is dominated by Arg M247, which has a pK_a shift of ~1 unit when Q_A is reduced. The remainder of the proton uptake associated with the reduction of Q_A results from small pK_a shifts of residues that individually change their average protonation by <0.2 protons. Previous calculations for the proton uptake associated with the reduction of Q_A (Gunner and Honig, 1992) exceed those presented here by as much as 0.2 protons; fluctuations (sampling noise) of this amount may be responsible for the discrepancy (see Fig. 2 in Gunner and Honig, 1992).

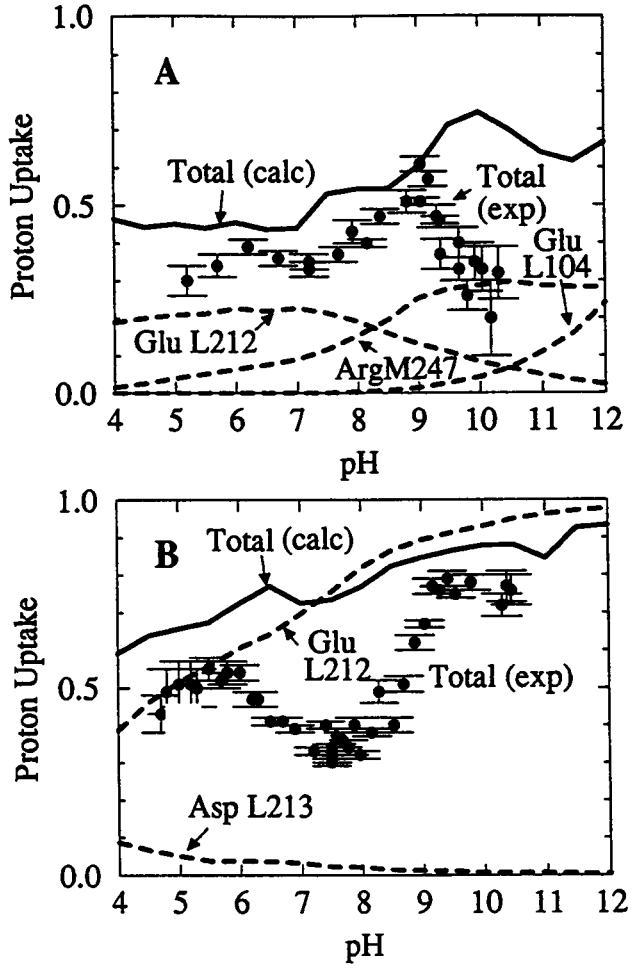

FIGURE 4 Calculated (———) and experimental (●) values for the proton uptake associated with the reduction of Q_A (*A*) and Q_B (*B*). Individual contributions to the calculated proton uptake from residues whose protonation changed by >0.1 protons are also shown (---). Calculated total proton uptake (———) was obtained by evaluating Eq. 9 every 0.5 pH units. Contributions from individual residues were obtained every 0.5 pH units from the difference in Eq. 6 for the two quinone redox states. Experimental values are from McPherson et al. (1988).

Proton uptake associated with reduction of Q_B

The calculated proton uptake associated with reduction of Q_B is shown in Fig. 4 *B*. The proton uptake is dominated by Glu L212, which was calculated to titrate gradually, starting at low pH. It accounts for all of the proton uptake above pH 5. At lower pH, Asp L213 makes a small contribution. Previous calculations of the proton uptake associated with the reduction of Q_B are also dominated by the protonation changes of Glu L212. However, the calculated proton uptake at low pH was higher than that presented here, because Glu L212 was calculated to have a lower pK_a (Gunner and Honig, 1992), which causes a larger proton uptake at low pH when Q_B is reduced.

Review of experimental results

Proton uptake by RCs in response to the reduction of Q_A and Q_B has been measured experimentally by monitoring the so-

lution pH, which changes as protons are withdrawn from solution by RCs (Maroti and Wraight, 1988; McPherson et al., 1988; Shinkarev et al., 1992). The experimentally measured proton uptake was found to be pH dependent and was greater for reduction of Q_B than for Q_A (see Fig. 4 *B*). We compare our calculated results for proton uptake with those reported by McPherson et al. (1988), which have been corroborated by other workers (Shinkarev et al., 1992) and were found to agree with the independently measured pH dependence of the free energy $\Delta G(Q_A^- Q_B \rightarrow Q_A Q_B^-)$ (Kleinfeld et al., 1984) (see Eq. 10). The proton uptake values originally reported by Maroti and Wraight (1988) disagree significantly from those obtained more recently by the same group (Shinkarev et al., 1992). The reason for this discrepancy is not known (Shinkarev et al., 1992).

Comparison of computational and experimental results

The calculated proton uptake associated with reduction of Q_B is greater than that associated with the reduction of Q_A, in agreement with experiment. However, a quantitative agreement between the calculated and experimentally measured pH dependence of the proton uptake is obtained only over portions of the pH range (see Fig. 4).

The calculated proton uptake resulting from reduction of Q_A is in fair agreement with experiment for pH < 9. Most of the proton uptake is caused by small shifts in the average protonation of several residues that interact weakly with Q_A^-. As seen in Fig. 3 *A*, most residues near Q_A do not titrate and, therefore, will not undergo pK_a shifts that increase the net protonation of the RC. In fact, the largest contribution to the proton uptake in this pH range comes from the relatively distant Glu L212 (see Fig. 1). For pH > 9, there is significant disagreement between computed and experimental values for proton uptake. This appears to be the result of proton uptake by Arg M247, which was calculated to titrate at an anomalously low pH (see Fig. 3). Throughout the pH range of the calculation, a significant fraction of the proton uptake is from residues that undergo small (<0.2) shifts in average protonation (not shown in Fig. 4). This contrasts with the proton uptake for Q_B, which is dominated by nearby residues.

For reduction of Q_B, the agreement between calculated and experimental proton uptake is poorer than for reduction of Q_A. An interesting feature of the proton uptake associated with the reduction of Q_B is the lack of proton uptake by residues other than Glu L212, some of which interact strongly with Q_B^- (see Table 3), and hence one might expect these other residues to undergo pK_a shifts that would cause proton uptake. There are two reasons why this does not occur. First, many charged residues near Q_B interact strongly with oppositely charged residues. These interactions, which stabilize the ionized forms of the residues involved, cannot be overcome by the introduction of a new negative charge (Q_B^-) in the region. As a result, the protonation state of these residues does not change. Second, the protonation of Glu L212 buffers the effect of the negative charge on Q_B. Residues near Q_B that might undergo a pK_a shift after Q_B is reduced are also close to Glu L212, which is partially ionized. Thus, reduction of Q_B, which shifts pK_as up, is largely compensated by the protonation of Glu L212, which shifts pK_as down. It is important to note that it is necessary to treat the interactions among residues statistically to obtain correct results. If only pairwise interactions between the quinone and titrating sites are considered, and the interactions between residues are not taken into account, the proton uptake will be vastly overestimated, as pointed out by McPherson et al. (1988).

Although our calculations are in general agreement with those reported by Gunner and Honig (1992), neither calculation is in good agreement with experiment (McPherson et al., 1988; Shinkarev et al., 1992). Previous comparison between calculated and experimental proton uptake, which showed good agreement (Gunner and Honig, 1992), was based on experimental data (Maroti and Wraight, 1988) that have been superceded (Shinkarev et al., 1992). Thus, proton uptake calculated from the continuum electrostatic model gives only qualitative agreement with experiment.

FREE ENERGY OF ELECTRON TRANSFER

Computational results

The pH dependence of ΔG *determined from the calculated proton uptake*

The pH dependence of the free energy of electron transfer can be obtained, to within an arbitrary integration constant, by integrating the difference in proton uptake between $Q_A^- Q_B$ and $Q_A Q_B^-$ (see Eq. 10). This integral was calculated and the integration constant was chosen to give agreement with experiment at pH 7 (see Fig. 5).

ΔG *calculated from the equilibrium population of* $Q_A^- Q_B$

A second method of calculating the free energy of electron transfer between Q_A and Q_B is to treat the redox states of the quinones with the same continuum model that was used to calculate the titration curves for the amino acids. An intrinsic redox free energy was calculated for each quinone and the dimensions of the **W** matrix in Eq. 7 were increased to include interactions between the quinones and the titrating sites. Thus, the free energy associated with reduction of Q_A and Q_B is obtained in a manner similar to that used to obtain pK_a values. However, we are interested in differences in redox energy between Q_A^- and Q_B^-. Therefore, comparison of the electrostatic energy of the quinones to a reference state in solution (as was done for calculation of amino acid pK_a) is unnecessary (i.e., both Q_A and Q_B are ubiquinone-10 molecules, and any reference energy would be the same for Q_A and Q_B). As we are concerned with the equilibrium between $Q_A^- Q_B$ and $Q_A Q_B^-$, only these two redox states are considered in the statistics (i.e., the states Q_A Q_B and $Q_A^- Q_B^-$ are omitted).

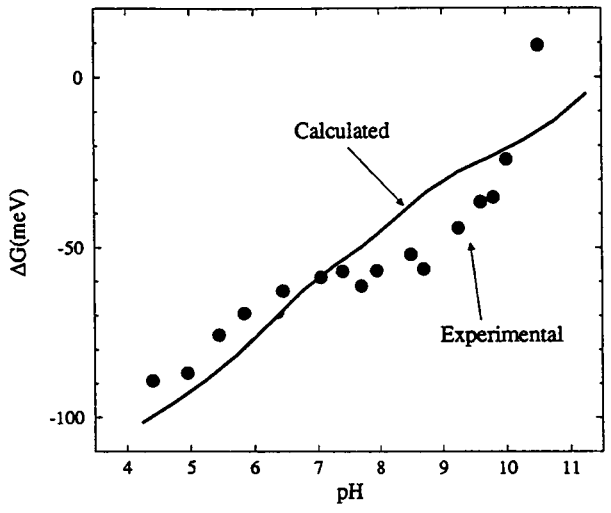

FIGURE 5 pH dependence of the free energy, ΔG, of electron transfer from Q_A to Q_B. The experimental curve was determined using Eq. 13 and the experimental values for k_{AD} and k_{BD} (Okamura and Feher, 1992). The calculated curve was obtained by integrating the calculated proton uptake, $\Delta[H^+](Q_A^-Q_B \rightarrow Q_AQ_B^-)$ (see Eq. 10), and the integration constant was chosen to give agreement with experiment at pH 7. The calculated value differs slightly from that reported previously (Beroza et al., 1991) because the charge distribution that represents the titrating amino acids has been improved (the previous calculation modeled a charged residue as a point charge, while the present calculation uses a more realistic charge distribution).

The change in free energy associated with electron transfer is separated into three parts:

$$\Delta G(Q_A^-Q_B \rightarrow Q_AQ_B^-) = \Delta G_{solv}(Q_A^-Q_B \rightarrow Q_AQ_B^-) + \Delta G_{bg}(Q_A^-Q_B \rightarrow Q_AQ_B^-) + \Delta G_{titr}(Q_A^-Q_B \rightarrow Q_AQ_B^-), \quad (17)$$

where the three terms, as in the case of amino acid pK_a shifts, represent solvation, background, and interaction energies with charged residues (note that ΔG_{titr} is used for notational convenience; as was the case with amino acid titration, the contribution from charged sites cannot be represented by a single number). The shifts in redox energy were calculated with the same continuum electrostatic model used for calculating amino acid titration.

ΔG_{solv}

The solvation energy arises from the interaction of the semiquinone with the polarization that it induces in the dielectric media (protein and solvent) and the redistribution of counterions it causes. Both quinone binding sites are out of contact with the aqueous solution and, therefore, have highly unfavorable solvation energies for the reduced form of the quinone (i.e., if only solvation effects are considered, it takes ~340 meV more energy to reduce a quinone bound to the RC than it does in solution). ΔG_{solv} is approximately the same for Q_A and Q_B, with a slight preference for the $Q_AQ_B^-$ state: $\Delta G_{solv}(Q_A^-Q_B \rightarrow Q_AQ_B^- = -26$ meV.

ΔG_{bg}

The background energy arises from interactions between the quinone and fixed charges and dipoles in the protein when all titrating sites are in their neutral state. The only fixed charge in the protein is on the iron-ligand complex (Fe^{2+}, an ionized glutamic acid, and four neutral histidines make a net charge of $+1e$). Other background charges are the dipole moments associated with the peptide bond and the polar sidechains of amino acid residues. These interactions strongly favor the reduction of both quinones by ~−450 meV. Thus, background interactions stabilize charge on either quinone. However, the stabilization is approximately the same for Q_A^- and Q_B^-; consequently, the effect of background interactions on the electron transfer equilibrium is small: $\Delta G_{bg}(Q_A^-Q_B \rightarrow Q_AQ_B^-) = +11$ meV. Again we see that the two quinone sites are remarkably equivalent. This is especially striking when one considers that the iron is closer to Q_B, and, therefore, preferentially stabilizes the $Q_AQ_B^-$ state.

The contributions to ΔG_{bg} of individual residues that have an interaction with the quinone of >50 meV are listed in Tables 7 and 8. The background energies resulting from the peptide bonds, ΔG_{bb}, and the amino acid sidechains, ΔG_{sc}, are separately listed. The largest background interactions are from the members of the iron/ligand complex (Fe^{2+}, Glu M234, His M219, His L190, His L230, and His M266), which have stronger interactions with Q_B than with Q_A. However, favorable interactions between Q_A and the dipoles of Thr M222 and Asn M259 help to counteract this effect.

From Tables 7 and 8, we see that residues that interact with the quinones by more than 50 meV contribute only about half of the total stabilization energy. The other half of the stabilization arises from longer-range interactions. As was seen for acidic residues near Q_B, peptide dipoles preferentially stabilize negative charge. Both Q_A and Q_B have favorable long-range interactions with the peptide dipoles, although they are not as strong as the interactions between the peptide dipoles and the acidic residues near Q_B.

ΔG_{titr}

Although the interactions with the nontitrating parts of the RC are similar for Q_A and Q_B, the interactions with titrating

TABLE 7 Q_A background interactions (meV)

Residue	ΔG_{bg}*	ΔG_{bb}‡	ΔG_{sc}§
Glu M234	114	4	110
His M219	−112	−2	−110
Fe¶	−93	–	−93
Thr M222	−86	−25	−61
Asn M259	−82	−55	−27
Ala M248	60	60	0
All others	−258	−101	−157
Total	−458	−119	−339

*Total background interaction with the residue.
‡Contribution to ΔG_{bg} from the polypeptide backbone.
§Contribution to ΔG_{bg} from the protein sidechains.
¶The non-heme iron was considered a sidechain atom.

TABLE 8 Q_B background interactions (meV)

Residue	ΔG_{bg}	ΔG_{bb}	ΔG_{sc}
His L190	-176	-14	-161
Glu M234	138	-3	141
Fe*	-123	-	-123
Ser L223	-90	-45	-45
His L230	-55	-1	-54
Gly L225	53	53	0
Thr L226	51	42	9
All Others	-247	-193	-55
Total	-449	-161	-288

*Heading definitions are the same as in Table 7.

residues are quite different. The strongest electrostatic interactions are listed in Tables 2 and 3.

As seen in Figs. 1 and 3, there are few charged residues near Q_A. Of those residues that have an interaction energy >50 meV, Arg M247 is the only one that is likely to be charged. On the other hand, Q_B interacts strongly with several acidic groups that were calculated to be charged in the experimental pH range. Titration curves for these residues are shown in Fig. 3, for neutral quinones. However, calculation of ΔG_{titr} must include the effect of proton uptake associated with the reduction of the quinones. As described earlier, if the electron states are sampled by the Monte Carlo method, the partition coefficient can be calculated, and the free energy of electron transfer can then be obtained from Eq. 11. This provides a direct calculation of the free energy, without the arbitrary integration constant that is needed when calculating the free energy from the integral of the proton uptake. The changes in protonation of residues associated with electron transfer between the quinones are taken into account in the Monte Carlo evaluation of Eq. 14.

As was the case for ΔG_{bg}, much of the contribution to ΔG_{titr} results from long-range interactions. For both quinones, the electrostatic influence of charged residues remains significant for the 25 nearest titrating sites. The ratio of charged cationic residues to charged anionic residues in the Q_A and Q_B regions is significantly different. Of the 25 closest titrating sites to Q_A, 11 of them are positively charged while only 6 of them are negatively charged (the remaining residues are neutral). This unbalanced charge distribution stabilizes negative charge on Q_A. Contrast this with the distribution of charged titrating sites near Q_B. Of the 25 nearest residues, 7 are positively charged and 9 are negatively charged. This charge distribution destabilizes negative charge on Q_B, i.e., it favors reduction of Q_A over Q_B. These two effects combine to give a free energy that ranges from +130 meV at low pH to +230 at high pH. Thus, the positive value for the free energy is the result of interactions with titrating sites.

Calculations on mutant RCs

The changes in the recombination rate, k_{BD}, resulting from site-specific mutations of residues near Q_B were calculated using the methods described in the previous section (see Eq. 13). Three acidic residues, Glu L212, Asp L213, and Asp L210 were mutated to neutral residues; calculated effects on k_{BD} of these mutations are shown in Fig. 6.

The Glu L212 → Gln mutant has the largest effect on the calculated recombination rate. When this residue is mutated to a neutral, non-titrating residue, less negative charge is near Q_B, which stabilizes the $Q_AQ_B^-$ state. Therefore, the recombination rate is slower (see Eq. 13). The largest decrease in rate is at high pH, because the glutamic acid in the wildtype is fully ionized. The Asp L213 → Asn mutant has no significant effect on the recombination rate. This is not surprising, because in the wildtype RC, Asp L213 was calculated to be almost fully protonated. Therefore, mutation to asparagine (which was modeled as a protonated aspartic acid) has little effect on the charge distribution. Of the three acids that were mutated, Asp L210 is the farthest from Q_B. The main effect of replacing this acid with a neutral one is to lower the pK_a of Glu L212. This in turn raises the energy of $Q_AQ_B^-$ at a lower pH than in the wildtype.

Review of experimental results

Two experimental methods have been used to measure the pH dependence of the free energy difference between $Q_A^-Q_B$ and $Q_AQ_B^-$. The first method relies on the integration of the experimentally observed proton uptake (see Fig. 4) as given by Eq. 10. This method gives the free energy only within an integration constant. The second method uses the rate of charge recombination (k_{BD}) between the secondary quinone (Q_B) and the bacteriochlorophyll dimer (the primary donor, D) as a probe for the free energy difference between the electron transfer states $Q_A^-Q_B$ and $Q_AQ_B^-$ (Kleinfeld et al.,

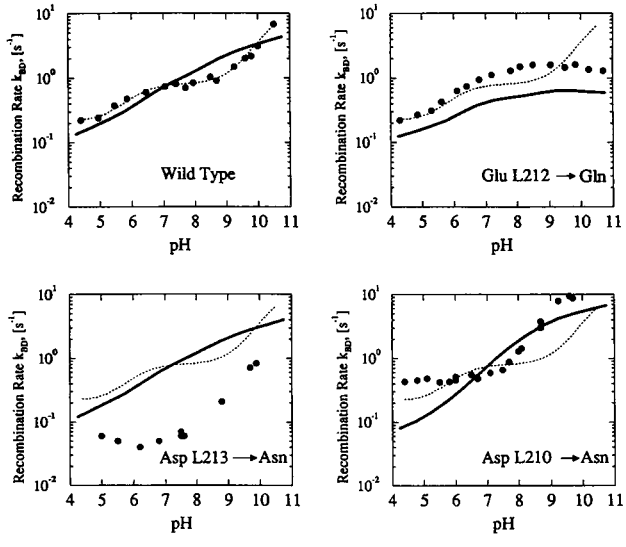

FIGURE 6 Computational (———) and experimental (●) recombination rate (k_{BD}) as a function of pH for native and mutant RCs. The experimental recombination rate for the wildtype (·····) is shown for each mutant for comparison. Experimental data from Okamura and Feher (1992).

1984). The charge recombination rate was shown to proceed indirectly by thermal population of the $Q_A^-Q_B$ state (Kleinfeld et al., 1984). Therefore, k_{BD} can be related, by Eq. 13, to $\Delta G(Q_A^-Q_B \rightarrow Q_AQ_B^-)$ and k_{AD} (i.e., the rate of $D^+Q_A \rightarrow DQ_A$), which was measured independently. Thus, the free energy difference between $Q_A^-Q_B$ and $Q_AQ_B^-$ can be probed by the charge recombination rate; the faster the recombination, the higher the free energy of the $Q_AQ_B^-$ state. The experimentally measured pH dependence of ΔG is shown in Fig. 5. (For experiments with differing detergents (lauryldimethylamine *N*-oxide and poly(etheleneglycol)) the high pH upturn in recombination rate shifts by ~1 pH unit (in lauryldimethylamine *N*-oxide the upturn occurs at pH ~ 10, in poly(etheleneglycol), the upturn occurs at pH ~ 9) We compare the theoretical calculations with the results for poly(ethelyeneglycol), which, unlike lauryldimethylamine *N*-oxide, is not a zwitterion, and, therefore, is more consistent with our solvent model.)

Experimental results for the charge recombination rate (k_{BD}) in wildtype and mutant RCs are shown in Fig. 6. The effect of these mutations on the charge recombination rate can be qualitatively understood in terms of an electrostatic interaction between Q_B^- and the titrating site that was mutated. These interactions and their implications for amino acid titration are summarized in Table 6.

Comparison of computational and experimental results

pH dependence of ΔG

The pH dependence of $\Delta G(Q_A^-Q_B \rightarrow Q_AQ_B^-)$ calculated from the proton uptake (Eq. 10) is compared with the experimentally determined pH dependence in Fig. 5. The calculated pH dependence of the free energy of electron transfer reproduces the general features of electrostatic coupling between the reduced quinones and titrating sites. The overall change in free energy of ~100 meV over the experimental pH range is reproduced reasonably well by the calculation. The shape of the calculated curve is mainly the result of the proton uptake of Glu L212. Glu L212 protonates fully when Q_B is reduced, and the energy required for this protonation increases with increasing pH (i.e., the work required to remove a proton from solution increases as the proton concentration in solution decreases).

The value of ΔG

The absolute free energy change associated with electron transfer from Q_A to Q_B, which was calculated from the equilibrium population of the $Q_A^-Q_B$ state, is higher than the experimentally measured value by ~230 meV. Since the solvation and background interactions are nearly the same for both quinones, the calculated unfavorable ΔG must result from interactions with charged residues. Which titrating sites are responsible for making Q_B^- energetically unfavorable? At first, it might appear that ionized acidic residues near Q_B are responsible. However, the closest acids, Glu L212 and Asp L213, are protonated when Q_B is reduced. Asp L213 is protonated regardless of whether Q_A or Q_B is reduced, while Glu L212 is partially ionized until Q_B is reduced (this protonation gives rise to the pH dependence of the free energy). Although there is an energetic cost associated with protonating Glu L212, it is small. Consider the electron transfer at pH 7. At this pH, before electron transfer, the energy difference between the protonated and unprotonated forms of Glu L212 is small. After Q_B is reduced, the equilibrium is shifted, but at little energetic cost. Indeed, if Glu L212 is restricted to be protonated in the Monte Carlo sampling, the free energy of forward electron transfer is only lowered by 16 meV.

The cause of the calculated energy difference between $Q_A^-Q_B$ and $Q_AQ_B^-$ becomes clear when more distant titrating sites are taken into account. As discussed earlier, the distribution of nearby ionized residues is significantly different for Q_A and Q_B. The 25 closest residues to Q_A have a net charge of +5, while the 25 closest residues to Q_B have a net charge of −2. This unbalanced distribution of charged residues favors reduction of Q_A and is the principle factor in the calculation that makes forward electron transfer unfavorable.

The result for the electrostatic free energy of electron transfer between the quinones raises a puzzle. Experimentally we know that the forward electron transfer $Q_A^-Q_B \rightarrow Q_AQ_B^-$ proceeds, yet our calculations predict that the $Q_A^-Q_B$ state is stabilized by ~170 meV.

To account for this failure of the electrostatic model to predict the observed forward electron transfer, we must invoke either the possibility that non-electrostatic contributions to the energy of Q_A or Q_B are of importance or alternatively, that the electrostatic model we have used is inadequate. These possibilities are discussed in the next section.

DISCUSSION

Relevance of the calculations to RC function

Stabilization of negative charge

One of the main results of the calculations is that near the quinones negative charges are preferentially stabilized over positive charges by the RC structure. The positively charged iron complex provides some of this stabilization. Less obvious is the contribution of the permanent dipoles of the polypeptide backbone of the RC, which are oriented to stabilize negative charge near the quinone sites, especially near Q_B. As pointed out by Gunner and Honig (1992), this structural feature is important for stabilizing the acidic residues near Q_B, which have the unique property of being poorly solvated and not involved in salt bridges with positively charged residues. Because the quinones are embedded in a low dielectric medium and far removed from solvent, the presence of an extra electron on a quinone is an energetic liability. Compensation for this loss of solvation is one of the important functions of the RC; the unfavorable solvation energy for a reduced

quinone at either Q_A or Q_B is compensated for by background interactions with the RC.

Anomalous titrations

A second result of this work is the unusual shape of the titration curves that were calculated for residues near the quinones. All residues that interact strongly with the quinones and that titrate in the experimental pH range had titration curves that cannot be described by the classical Henderson-Hasselbach equation (see Fig. 3). In the case of Glu L212 or Asp L210, deprotonation with increasing pH occurs over a much larger range than expected. In the case of Asp L213, the difference is more severe; the protonation increases with increasing pH. Although some of these results are likely to be the result of the simplifying assumptions of the model (see below), the gradual titration of Glu L212 has some experimental backing. Titration of Glu L212 over a large pH range helps to explain the two seemingly conflicting experimental results for the pK_a (Paddock et al., 1989; Hienerwadel et al., 1995).

Coupling of proton and electron transfer

The calculated proton uptake (Fig. 4), and the resulting pH dependence of the free energy (Fig. 5), associated with electron transfer between Q_A and Q_B demonstrates quantitatively how proton uptake results from pK_a shifts induced by the electrostatic interaction with the electron. However, it is not sufficient to treat only the pairwise interactions between the reduced quinone and the titrating sites. To obtain valid results, the interactions between titrating sites must be included. This significantly reduces the effect of quinone reduction on the protonation state of nearby titrating sites. This can be seen by examining the interactions between Q_B and nearby titrating sites in Table 3. The interactions between the quinone and the closest acidic residues are large enough to cause several of these residues to have significant proton uptake. Instead, only Glu L212 protonates, and for other residues the upward pK_a shift caused by reduction of Q_B is compensated for by a downward pK_a shift caused by the protonation of Glu L212.

Limitations of the continuum model

The electrostatic model used in these calculations relies on a number of simplifying assumptions (described earlier). Relaxing these assumptions and refinements of the model should improve the calculations. Several of these are discussed below.

Neglect of protein motion may be a significant source of error. When either quinone is reduced, a negative charge is introduced in a deeply buried region of the RC. The large electrostatic forces that result are likely to cause reorientation of polar sidechains. Molecular dynamics studies of earlier stages of electron transfer in the RC have shown that protein rearrangement can contribute as much as 400 meV to the electron transfer energy (Treutlein et al., 1992), although bulk solvent was not included in the calculation. In the continuum electrostatic model, such relaxation is incorporated in the dielectric constant of the protein, which may underestimate the effect of reorientation of permanent dipoles, especially at short distances. Moreover, molecular dynamics simulation of the free energy of electron transfer between the quinones has shown good agreement with experiment (Nonella and Schulten, 1994), despite the assumption that Glu L212 remains ionized after electron transfer to Q_B, which is contrary to experimental evidence and would inhibit forward electron transfer.

The modeling of the protein as a dielectric continuum raises some questions. Is it correct to model interactions on the atomic level with continuum electrostatic theory? If so, what is the proper choice for the protein dielectric constant? It has been shown that a much higher protein dielectric constant ($\sim$20) gives better results for pK_a values of amino acids in globular proteins (Antosiewicz et al., 1994), although it is likely that this high value compensates for other effects that are not included in the continuum electrostatic model (i.e., protein motion and ion binding).

Structural features unique to the RC may also be a target for more accurate modeling with the continuum electrostatic theory. There are internal voids, which probably contain bound water molecules, near Q_B (Beroza et al., 1992). These internal cavities are accessible to the spherical probe that is used to define the molecular surface of the protein and are, therefore, assigned a high dielectric constant. Modeling these internally bound water molecules as volumes of high dielectric may not be sufficiently accurate. In preliminary studies we found that the orientation of nearby water molecules changes the protonation state of Asp L213. Other workers have found that the orientation of explicit water molecules can greatly alter the pK_a values obtained from continuum electrostatic calculations (Yang et al., 1993; Sampogna and Honig, 1994).

Finally, a complete description of energetics should include non-electrostatic contributions to the quinone redox energies. For example, the electronic states of a quinone may be altered by interactions with the protein matrix. Any interaction that affects Q_A and Q_B differently would affect the free energy difference between $Q_A^- Q_B$ and $Q_A Q_B^-$ but would not show up in an electrostatic calculation.

CONCLUSIONS

We have applied a continuum electrostatic model to investigate the coupling of electron and proton transfer in the photosynthetic RC. Thermal averages of protonation of amino acids and electron transfer states were computed using Monte Carlo sampling, and modified sampling techniques were employed to improve sampling efficiency.

An important result of this work relates to the titration of amino acids that are near the quinone binding sites, especially those near Q_B. These residues have strong interactions with each other that give rise to titration curves that do not obey the classical Henderson-Hasselbach change in proto-

nation with pH. Our results show that the titration of strongly interacting residues can be complicated. This may be particularly relevant for the titration of Glu L212, for which we calculated a gradual titration curve, with partial ionization over a large pH range. This gradual titration provides a working model to reconcile the experimental results, one that is consistent with an unusually high pK_a for Glu L212 of ~9.5 (Paddock et al., 1989) and one that is consistent with a more standard pK_a for Glu L212 of ~4.5 (Hienerwadel et al., 1995). In light of the results presented here, we suggest that the interpretation of these experimental results in terms of classical titration curves, characterized by a single pK_a value, is inadequate.

The calculated pH dependence of the free energy difference between $Q_A^- Q_B$ and $Q_A Q_B^-$ shows how electrostatic coupling between the electron and the titrating amino acids in the RC affects electron transfer energetics. However, the coupling is more complex than can be explained using classical ideas of pK_a and pK_a shifts induced by interactions with the reduced quinones. The interactions between titrating sites tend to counteract the effect of changes in the redox state of the quinone, especially in the Q_B region, where the protonation of Glu L212 essentially cancels the effect of the reduction of Q_B. Thus, other titrating sites are not as affected by the charge on the quinone as one would expect from the pairwise interaction between the reduced quinone and the titrating site (as in Table 3).

The discrepancies between calculated and experimental values for titration curves of individual residues and the free energy difference between the $Q_A^- Q_B$ and $Q_A Q_B^-$ states suggest that the continuum electrostatic model lacks important factors that are needed to determine electron transfer energetics, and we suggest that conformational rearrangement of the protein in response to electron transfer is the most important.

We thank Donald Bashford, Marilyn Gunner, Louis Noodleman and Charles Perrin for helpful discussions. This work was supported by National Institutes of Health grant GM13191 (GF) and NIH training grant GM08326 (PB).

REFERENCES

Allen, J. P., G. Feher, T. O. Yeates, H. Komiya, and D. C. Rees. 1987a. Structure of the reaction center from *Rhodobacter sphaeroides* R-26: the protein subunits. *Proc. Natl. Acad. Sci. USA.* 84:6162–6166.

Allen, J. P., G. Feher, T. O. Yeates, H. Komiya, and D. C. Rees. 1987b. Structure of the reaction center from *Rhodobacter sphaeroides* R-26: the cofactors. *Proc. Natl. Acad. Sci. USA.* 84:5730–5734.

Antosiewicz, J., J. A. McCammon, and M. K. Gilson. 1994. Prediction of pH-dependent properties of proteins. *J. Mol. Biol.* 238:415–436.

Bashford, D., and K. Gewert. 1992. Electrostatic calculations of the pK_a values of ionizable groups in bacteriorhodopsin. *J. Mol. Biol.* 224:473–486.

Bashford, D., and M. Karplus. 1990. pK_as of ionizable groups in proteins: atomic detail from a continuum electrostatic model. *Biochemistry.* 29: 10219–10225.

Bashford, D., and M. Karplus. 1991. Multiple-site titration curves of proteins: an analysis of exact and approximate methods for their calculation. *J. Phys. Chem.* 95:9556–9561.

Bernstein, F. C., T. F. Koetzle, G. J. B. Williams, E. F. Meyer Jr., M. D. Brice, J. R. Rodgers, O. Kennard, T. Shimanouchi, and M. Tasumi. 1977. The Protein Data Bank: a computer-based archival file for macromolecular structures. *J. Mol. Biol.* 112:535–542.

Beroza, P., D. R. Fredkin, M. Y. Okamura, and G. Feher. 1991. Protonation of interacting residues in a protein by a Monte Carlo method: application to lysozyme and the photosynthetic reaction center of *Rhodobacter sphaeroides*. *Proc. Natl. Acad. Sci. USA.* 88:5804–5808.

Beroza, P., D. R. Fredkin, M. Y. Okamura, and G. Feher. 1992. Proton transfer pathways in the reaction center of *Rb. sphaeroides*: a computational study. *In* The Photosynthetic Bacterial Reaction Center II. J. Breton and A. Verméglio, editors. Plenum Press, New York. 363–374.

Beroza, P., D. R. Fredkin, M. Y. Okamura, and G. Feher. 1994. Calculating the pK_a of Glu L212 in the photosynthetic reaction center: sensitivity of the results to variation of parameters. *Biophys. J.* 66:A229.

Chandler, D. 1987. Introduction to Modern Statistical Mechanics. Oxford University Press, New York.

Connolly, M. L. 1983. Analytical molecular surface calculation. *J. Appl. Cryst.* 16:548–558.

Cramer, W. A., and D. B. Knaff. 1990. Energy Transduction in Biological Membranes. Springer-Verlag, New York.

Crofts, A. R., and C. A. Wraight. 1983. The electrochemical domain of photosynthesis. *Biochim. Biophys. Acta.* 726:149–185.

Davis, M. E., and J. A. McCammon. 1990. Electrostatics in biomolecular structure and dynamics. *Chem. Rev.* 90:509–521.

Feher, G., M. L. Paddock, S. H. Rongey, and M. Y. Okamura. 1992. Proton transfer pathways in photosynthetic reaction centers studied by site-directed mutagenesis. *In* Membrane Proteins: Structure, Interactions, and Models, Vol. 125. A. Pullman, J. Jortner, B. Pullman, editors. Kluwer Academic Publishers, Dordrecht. 481–495.

Gilson, M. K. 1993. Multiple-site titration and molecular modeling: two rapid methods for computing energies and forces for ionizable groups in proteins. *Proteins.* 15:266–282.

Gilson, M. K., and B. H. Honig. 1986. The dielectric constant of a folded protein. *Biopolymers.* 25:2097–2119.

Gilson, M. K., and B. H. Honig. 1988. Energetics of charge-charge interactions in proteins. *Proteins.* 3:32–52.

Gunner, M. R., and B. Honig. 1992. Calculations of proton uptake in *Rhodobacter sphaeroides* reaction centers. *In* The Photosynthetic Bacterial Reaction Center II. J. Breton and A. Verméglio, editors. Plenum Press, New York. 403–410.

Hagler, A. T., E. Huler, and S. Lifson. 1974. Energy functions for peptides and proteins. I. derivation of a consistent force field including the hydrogen bond from amide crystals. *J. Am. Chem. Soc.* 96:5319–5327.

Harvey, S. C. 1989. Threatment of electrostatic effects in molecular modeling. *Proteins.* 5:78–92.

Hienerwadel, R., S. Grzybek, C. Fogel, W. Kreutz, M. Y. Okamura, M. L. Paddock, J. Breton, E. Nabedryk, and W. Mäntele. 1995. Protonation of Glu L212 following Q_B^- formation in the photosynthetic reaction center of *Rhodobacter sphaeroides*: direct evidence from time-resolved infrared spectroscopy. *Biochemistry.* 34:2832–2843.

Kleinfeld, D., M. Y. Okamura, and G. Feher. 1984. Electron transfer in reaction centers of *Rhodopseudomonas sphaeroides*. I. Determination of the charge recombination pathway of $D^+Q_AQ_B^-$ and free energy and kinetic relations between $Q_A^-Q_B$ and $Q_AQ_B^-$. *Biochim. Biophys. Acta.* 766:126–140.

Maroti, P. and C. A. Wraight. 1988. Flash-induced H^+ binding by bacterial photosynthetic reaction centers: comparison of spectrophotometric and conductimetric methods. *Biochim. Biophys. Acta.* 934:314–328.

McPherson, P. H., M. Y. Okamura, and G. Feher. 1988. Light-induced proton uptake by photosynthetic reaction centers from *Rhodobacter sphaeroides* R-26. I. Protonation of the one-electron states $D^+Q_A^-$, DQ_A^-, $D^+Q_AQ_B^-$, and $DQ_AQ_B^-$. *Biochim. Biophys. Acta.* 934: 348–368.

McPherson, P. H., M. Y. Okamura, and G. Feher. 1990. Electron transfer from the reaction center of *Rb. sphaeroides* to the quinone pool: doubly reduced Q_B leaves the reaction center. *Biochim. Biophys. Acta.* 1016: 289–292.

McQuarrie, D. 1976. Statistical Mechanics. Harper and Row, New York.

Nonella, M., and K. Schulten. 1994. Molecular dynamics simulation of electron transfer in proteins. Theory and application to $q_a \rightarrow q_b$ transfer

in the photosynthetic reaction center. *J. Phys. Chem.* 98:1978–1988.

Oberoi, H., and N. M. Allewell. 1993. Multigrid solution of the nonlinear Poisson-Boltzmann equation and calculation of titration curves. *Biophys. J.* 65:48–55.

Okamura, M. Y., and G. Feher. 1992. Proton transfer in reaction centers from photosynthetic bacteria. *Annu. Rev. Biochem.* 61:861–896.

Paddock, M. L., G. Feher, and M. Y. Okamura. 1990. pH dependence of charge recombination in RCs from *Rb. sphaeroides* in which Glu-L212 is replaced with Asp. *Biophys. J.* 57:569a.

Paddock, M. L., A. Juth, G. Feher, and M. Y. Okamura. 1992. Electrostatic effects of replacing Asp-L210 with Asn in bacterial RCs from *Rb. sphaeroides. Biophys. J.* 61:153a.

Paddock, M. L., S. H. Rongey, G. Feher, and M. Y. Okamura. 1989. Pathway of proton transfer in bacterial reaction centers: replacement of glutamic acid 212 in the L subunit by glutamine inhibits quinone (secondary acceptor) turnover. *Proc. Natl. Acad. Sci. USA.* 86:6602–6606.

Richards, F. M. 1977. Areas, volumes, packing, and protein structure. *Annu. Rev. Biophys. Bioeng.* 6:151–176.

Sampogna, R., and B. Honig. 1994. Environmental effect on the protonation states of active site residues in bacteriorhodopsin. *Biophys. J.* 66:1341–1352.

Sharp, K., and B. Honig. 1990. Electrostatic interactions in macromolecules: theory and application. *Annu. Rev. Biophy. Biophys. Chem.* 19:301–332.

Shinkarev, V. P., E. Takahashi, and C. A. Wraight. 1992. Electrostatic interactions and flash-induced proton uptake in reaction centers from *Rb. sphaeroides*. *In* The Photosynthetic Bacterial Reaction Center II. J. Breton and A. Verméglio, editors. Plenum Press, New York. 375–387.

Sitkoff, D., K. A. Sharp, and B. Honig. 1994. Accurate calculation of hydration free energies using macroscopic solvent models. *J. Phys. Chem.* 98:1978–1988.

Sudmeier, J. L., and C. N. Reilly. 1964. Nuclear magnetic resonance studies of protonation of polyamine and aminocarboxylate compounds in aqueous solution. *Anal. Chem.* 36:1698–1706.

Takahashi, E., and C. A. Wraight. 1992. Proton and electron transfer in the acceptor quinone complex of *Rhodobacter sphaeroides* reaction centers: characterization of site-directed mutants of the two ionizable residues, Glu^{L212} and Asp^{L213}, in the Q_B binding. *Biochemistry.* 31:855–866.

Tanford, C., and J. G. Kirkwood. 1957. Theory of protein titration curves. I. General equations for impenetrable spheres. *J. Am. Chem. Soc.* 79: 5333–5339.

Tanford, C., and R. Roxby. 1972. Interpretation of protein titration curves. Application to lysosyme. *Biochemistry.* 11:2192–2198.

Treutlein, H., K. Schulten, A. T. Brünger, M. Karplus, J. Deisenhofer, and H. Michel. 1992. Chromophore-protein interactions and the function of the photosynthetic reaction center: a molecular dynamics study. *Proc. Natl. Acad. Sci. USA.* 89:75–79.

Warwicker, J., and H. C. Watson. 1982. Calculation of the electric potential in the active site cleft due to α-helix dipoles. *J. Mol. Biol.* 157:671–679.

Warshel, A., and S. T. Russell. 1984. Electrostatic interactions in biological systems and in solution. *Q. Rev. Biophys.* 17:283–422.

Yang, A.-S., M. R. Gunner, R. Sampogna, K. Sharp, and B. Honig. 1993. On the calculation of pK_as in proteins. *Proteins.* 15:252–265.